© 2019. Published by The Company of Biologists Ltd | Journal of Cell Science (2019) 132, jcs234948. doi:10.1242/jcs.234948

RESEARCH ARTICLE

TNAP limits TGF-β-dependent cardiac and skeletal muscle fibrosis by inactivating the SMAD2/3 transcription factors

Benedetta Arnò[1,2,*], Francesco Galli[1,*], Urmas Roostalu[1,3], Bashar M. Aldeiri[1,4], Tetsuaki Miyake[5], Alessandra Albertini[1,6], Laricia Bragg[1], Sukhpal Prehar[7], John C. McDermott[5], Elizabeth J. Cartwright[7] and Giulio Cossu[1,‡]

ABSTRACT

Fibrosis is associated with almost all forms of chronic cardiac and skeletal muscle diseases. The accumulation of extracellular matrix impairs the contractility of muscle cells contributing to organ failure. Transforming growth factor β (TGF-β) plays a pivotal role in fibrosis, activating pro-fibrotic gene programmes via phosphorylation of SMAD2/3 transcription factors. However, the mechanisms that control de-phosphorylation of SMAD2 and SMAD3 (SMAD2/3) have remained poorly characterized. Here, we show that tissue non-specific alkaline phosphatase (TNAP, also known as ALPL) is highly upregulated in hypertrophic hearts and in dystrophic skeletal muscles, and that the abrogation of TGF-β signalling in TNAP-positive cells reduces vascular and interstitial fibrosis. We show that TNAP colocalizes and interacts with SMAD2. The TNAP inhibitor MLS-0038949 increases SMAD2/3 phosphorylation, while TNAP overexpression reduces SMAD2/3 phosphorylation and the expression of downstream fibrotic genes. Overall our data demonstrate that TNAP negatively regulates TGF-β signalling and likely represents a mechanism to limit fibrosis.

KEY WORDS: SMAD, TGF-β receptor, Tissue non-specific alkaline phosphatase, ALPL, Striated muscle fibrosis, Cardiac hypertrophy, Muscular dystrophy

INTRODUCTION

Fibrosis accompanies many chronic diseases and is a common response to injury. It is characterized by excessive production, and accumulation of, collagen and other extracellular matrix (ECM) components, cellular dysfunction and loss of tissue architecture that eventually lead to organ failure (Ueha et al., 2012). Fibrosis can affect many organs, including heart and skeletal muscle, and has become a major cause of death in the developed world.

Fibrosis is an integral component of most cardiac pathological conditions and can be associated with cardiomyocyte death (Frangogiannis, 2012), pressure or volume overload (Berk et al., 2007), hypertrophic cardiomyopathy (Kania et al., 2009) and toxic insults (Bernaba et al., 2010).

Skeletal muscle fibrosis accompanies ageing, in which case gradual muscle loss leads to the accumulation of adipose tissue and ECM (Alnaqeeb et al., 1984; Wood et al., 2014). Fibrosis occurs early in congenital muscular dystrophies and impairs muscle function and regeneration (Serrano and Muñoz-Cánoves, 2017; Tedesco and Cossu, 2012). In both cardiac and skeletal muscle, fibrosis increases the stiffness of the tissue, thereby directly impairing muscle cell contraction.

The molecular pathways involved in fibrosis are well known and common for the two organs. Transforming growth factor β (TGF-β), in addition to being a major morphogen during development, is one of the main signalling molecules initiating fibrosis and is secreted by many cell types in the injured tissue. Its activity is controlled by proteolytic cleavage of a precursor, previously bound to inhibitory proteins and subsequently released by proteases. Active TGF-β binds to the serine threonine protein kinases receptors (termed TGF-β receptor type I and type II) and induces the phosphorylation and activation of SMAD2 and SMAD3 (SMAD2/3) transcription factors (also known as receptor-regulated SMADs or R-SMADs) (Heldin et al., 1997; Zi et al., 2012). The phosphorylation of R-SMADs triggers their association with SMAD4, leading to their nuclear translocation, where they control the transcription of pro-fibrotic genes. Finally, the dephosphorylation of R-SMADs promotes their exit from the nucleus and the end of the signalling (Bruce and Sapkota, 2012). As a central regulator of a number of physiologically important processes, TGF-β signalling is highly regulated. Cellular susceptibility is determined by receptor endocytosis via clathrin- and caveolin-dependent pathways (Di Guglielmo et al., 2003). Depletion of TGF-β ligand defines the transcriptional response and is achieved by TGF-β binding to the cell surface or its cellular uptake (Clarke et al., 2009). The duration and temporal dynamics of ligand availability influence downstream signalling response, as repeated pulses of TGF-β can lead to long-term sustained response (Zi et al., 2011). Several post-translational modifications are capable of regulating R-SMAD activity. These include ubiquitylation (Dupont et al., 2012, 2005; Episkopou et al., 2001; Lin et al., 2000; Zhu et al., 1999), acetylation (Grönroos et al., 2002), parpylation (Lönn et al., 2010), sumoylation (Miles et al., 2008) and phosphorylation at different serine residues (Kretzschmar et al., 1997). Rapid inactivation of R-SMADs can be achieved by dephosphorylation. However, to date only one R-SMAD phosphatase, protein phosphatase 1A (PPM1A), has been identified for the TGF-β pathway (Lin et al., 2006). Identification of new R-SMAD phosphatases would enable efficient attenuation of pro-fibrotic signalling in acute and chronic diseases.

Tissue non-specific alkaline phosphatase (TNAP, also known as ALPL) is an enzyme that is widely expressed in many organs. It is

[1]Division of Cell Matrix Biology & Regenerative Medicine, Faculty of Biology, Medicine and Health, University of Manchester, Manchester M13 9PT, UK. [2]Medicines Discovery Catapult, Mereside, Alderley Edge SK104TG, UK. [3]Gubra Hørsholm Kongevej 11B 2970 Hørsholm, Denmark. [4]King's College Hospital, Denmark Hill, London SE5 9RS, UK. [5]Department of Biology, York University, Toronto, ON, M3J 1P3, Canada. [6]TIGET-HSR, Ospedale San Raffele, Via Olgettina 60, 20132 Milan, Italy. [7]Division of Cardiovascular Sciences, Manchester Academic Health Science Centre, The University of Manchester, Manchester M13 9PT, UK.
*These authors contributed equally to this work

‡Author for correspondence (giulio.cossu@manchester.ac.uk)

F.G., 0000-0002-6696-4086; U.R., 0000-0002-7849-2055; G.C., 0000-0001-5863-9593

Received 31 May 2019; Accepted 27 June 2019

Journal of Cell Science (2019) 132, jcs234948. doi:10.1242/jcs.234948

involved in bone mineralization and mutations in the TNAP-encoding gene have been associated with hypophosphatasia, a rare inherited disorder, characterized by defective bone mineralization (Mornet et al., 2001). Recently TNAP has been associated with vascular calcification (Romanelli et al., 2017; Sheen et al., 2015) and cardiac fibro-calcification (Herencia et al., 2015). Its role in fibrosis and in the context of TGF-β signalling has not been addressed.

In the present study, we demonstrate that TNAP negatively regulates TGF-β signalling pathway by regulating the level of phosphorylation of SMAD2/3. We show that TNAP is highly induced in hypertrophic hearts and dystrophic skeletal muscle, and that the abrogation of TGF-β signalling in TNAP-positive cells reduces vascular and interstitial fibrosis. TNAP interacts with SMAD2 and its overexpression decreases SMAD phosphorylation and the expression of downstream fibrotic genes.

RESULTS

We previously established TNAP expression in skeletal muscle and demonstrated that its high activity marks perivascular cells (Dellavalle et al., 2007). In contrast, we found that TNAP is more widely expressed in healthy mouse heart. We detected alkaline phosphatase activity mainly in the interstitium (Fig. 1A,B) but also in cardiomyocytes (Fig. 1C). At higher resolution (Fig. 1D) AP activity colocalized both with endothelial (VE-cadherin^{+}) and perivascular (NG2^{+}) cells and also extended outside of the small vessels (Fig. 1D). Of the three alkaline phosphatase isoforms, intestinal (ALPI), embryonic (ALPG) and non-specific (TNAP), only the latter is expressed in the heart at any developmental stage examined (Fig. 1E). When TNAP-Cre^{ERT} mice (Dellavalle et al., 2011) were crossed to the *Rosa26NZG* reporter mice, LacZ activity was detected in many areas of the heart (Fig. 1F). Additional examples of TNAP localization in adult healthy heart are shown in Fig. S1.

Angiotensin II infusion increases TNAP expression in cardiomyocytes and cardiac fibroblasts *in vivo*

We next analysed changes in TNAP activity in response to fibrosis. We used a model of angiotensin II-induced cardiac hypertrophy, which is known to cause fibrosis after few days (Crowley et al., 2006). We implanted subcutaneous mini-pumps releasing angiotensin II (Ang II) (2.8 mg/kg of body weight per day) for 2 weeks in 10-week-old C57/BL6J mice. We analysed the hearts of treated mice for the presence of hypertrophy and fibrosis. As expected, the treatment with Ang II caused cardiomyocyte hypertrophy and led to an increase in tenascin C-positive areas compared with mice treated with saline solution (Sham) (Fig. S2a–i). Moreover, the expression of the fibrotic genes Fibronectin 1 (*Fn1*), tenascin C (*Tnc*), smooth muscle actin (*Sma*, also known as *Acta2*), vimentin (*Vim*) and collagen 1a2 (*Col1a2*) was significantly upregulated in Ang II-treated mice compared with the control (Fig. S2j–p).

We took advantage of this disease model to analyse the expression of *Tnap*. Interestingly, we found a significant increase in the number of TNAP-positive cells in hypertrophic hearts in comparison to the control (Fig. 2A–C; n=5 for each group). Moreover, we detected an upregulation of *Tnap* expression by quantitative (q)RT-PCR (Fig. 2D). In order to understand which cell types express TNAP in physiological and pathological conditions, we stained the heart sections for TNAP and laminin, vimentin and PECAM, which allow identification of cardiomyocytes basal lamina, cardiac interstitial and endothelial cells, respectively, and using confocal microscopy, counted the number of double-positive cells in a 77 mm^2 area. We confirmed that all three cells types analysed expressed TNAP in normal heart (TNAP/PECAM^{+} cells, 16.6±6%; TNAP/laminin^{+} cells, 26±5.4%; TNAP/vimentin^{+}/PECAM^{-}, cells 27±5.6%; n=3 mice, mean±s.d.). Remarkably, in the Ang II-treated mice the number of cells expressing TNAP significantly increased in all three different cell populations (TNAP^{+}/PECAM^{+} cells, 30.5±4.1%; TNAP^{+}/laminin^{+} cells, 42.4±1.5%; TNAP^{+}/vimentin^{+}/PECAM^{-} cells, 49.3±6%; n=3 mice, mean±s.d., P<0.001, two-tailed t-test) (Fig. 2E–M). These data prove that in hypertrophic hearts TNAP is significantly up regulated in cardiac myocytes, endothelial cells and interstitial cells.

However, it is important to notice that, under normal condition only a minority of cells in the heart express TNAP and even if this number almost doubles in the Ang II-treated animals, it remains confined to less than half of total cardiac cells.

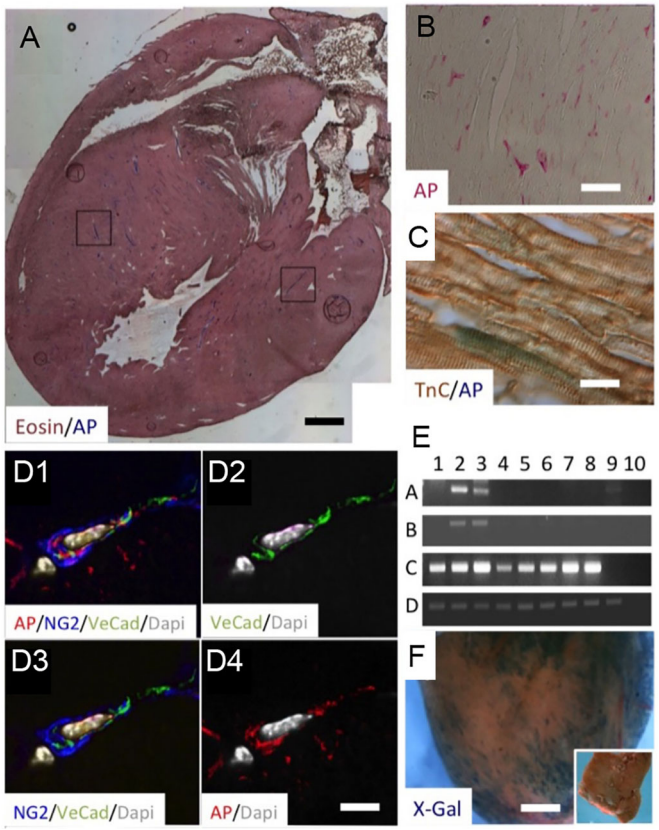

Fig. 1. TNAP activity under healthy, physiological conditions. (A–C) Frontal section of an adult [postnatal day (P)30] mouse heart stained for AP activity and eosin. AP activity is high in small and medium size vessels (squares in A) and is also observed in some cardiomyocytes (C). (D) Confocal triple immunofluorescence of a small vessel stained with anti-VE-cadherin (green) and anti-NG2 (blue) antibodies, and for AP activity (red). (E) RT-PCR with probes specific for embryonic (labelled A), intestinal (labelled B), tissue non-specific (labelled C) alkaline phosphatase and for GAPDH (labelled D). 1, adult liver; 2, adult intestine; 3, adult testis; 4, embryonic heart (E 11.5); 5, fetal heart (E 16.5); 6, neonatal heart (P1); 7, juvenile heart (P15); 8: adult heart (P90); 9, D16 (a line of embryonic mesoangioblasts; Minasi et al., 2002); 10, negative control. (F) TNAP activity is maintained in adulthood. Tamoxifen was injected for 3 consecutive days in TNAP-Cre^{ERT}×Rosa NGZ mice at P6, 7 and 8 and the heart was collected at P60 (Dellavalle et al., 2011). A control injection of oil is shown in the inset. Scale bars: 1 mm (A), 50 µm (B,C); 15 µm (D); 0.5 mm (F).

Journal of Cell Science (2019) 132, jcs234948. doi:10.1242/jcs.234948

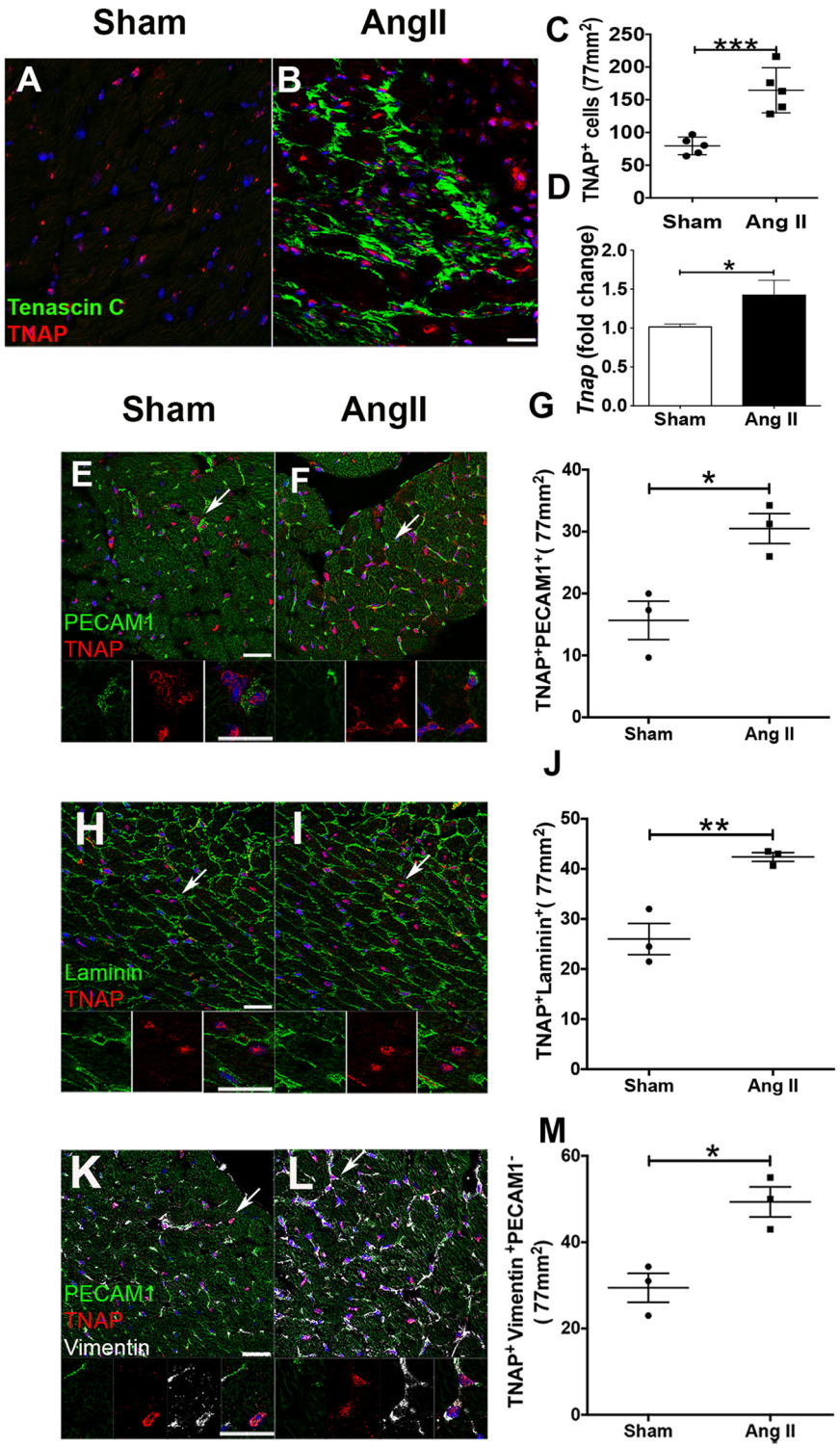

Fig. 2. TNAP is upregulated in different cell types during Ang II-induced fibrosis. (A,B) Immunofluorescence for tenascin C and TNAP in Sham- and Ang II-treated mice. (C) Quantification of the number of TNAP-positive cells for both samples (mean ±s.d., *n*=5). (D) qRT-PCR for *Tnap* in Sham- and Ang II-treated ventricle extracts (mean±s.d., *n*=5). (E–M) Confocal images of Sham- and Ang II-treated heart sections stained for TNAP and PECAM1 (E,F), TNAP and Laminin (H,I), and TNAP, PECAM1 and vimentin (K,L). The lower panels show high magnifications of double-positive cells (arrows in main images). Quantifications of the number of double-positive cells are indicated in G, J and M, respectively (mean±s.d., *n*=3). **P*<0.05, ***P*<0.01, ****P*<0.001 (two-tailed *t*-test). Scale bars: 20 µm.

The abrogation of TGF-β signalling in TNAP-positive cells reduces fibrosis in the heart and skeletal muscle

Since the increased number of TNAP-positive cells is preferentially localized in tenascin C-positive regions (Fig. 2A,B,K,L), we reasoned that TNAP-positive cells might have a role in the regulation of fibrosis upon Ang II treatment. TNAP is widely expressed in many different cells, so that creating a cardiac-specific knockout would be technically very challenging in this context as Cre should be driven by all least three (cardiac, endothelial and interstitial) different promoters. Therefore, to prove that TNAP-expressing cells are in fact involved in cardiac fibrosis, despite being a minority of total cardiac cells, we inactivated TGF-β signalling specifically in TNAP-positive cells. To achieve this goal, we took advantage of an inducible conditional knockout *Tnap*^{cre};*Tgfbr2* floxed mouse (Chytil et al., 2002; Dellavalle et al., 2011). This strain is characterized by the inactivation, upon tamoxifen injection, of TGF-β receptor 2 (TGF-βR2) in TNAP-expressing cells. We first verified by immunofluorescence whether TNAP-positive cells express

Journal of Cell Science (2019) 132, jcs234948. doi:10.1242/jcs.234948

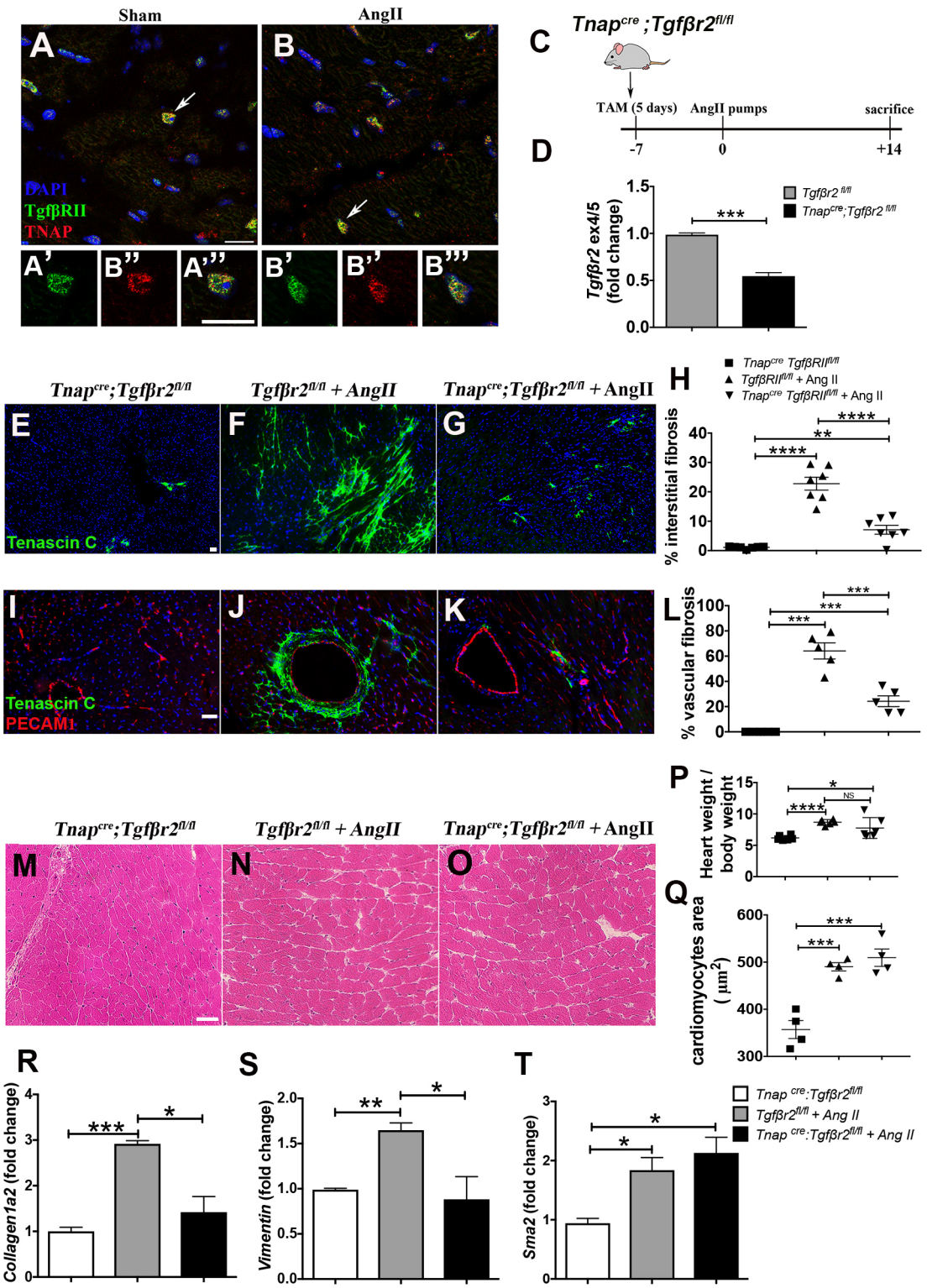

Fig. 3. See next page for legend.

TGF-βR2 and found that virtually all TNAP-positive cells are also positive for TGF-βR2, both in Sham- and Ang II-treated mice (Fig. 3A,B). We then injected the *Tnap*^{cre};*Tgfbr2*$^{fl/fl}$ transgenic mice with 100 mg/kg of body weight of tamoxifen once a day for 5 days; at day 7 we implanted subcutaneous mini-pumps releasing 2.8 mg/kg of body weight per day of Ang II for 2 weeks (Fig. 3C). We verified Cre recombination efficiency on the total heart of the *Tnap*^{cre};*Tgfbr2*$^{fl/fl}$ mice by qRT-PCR for the exon 4 of the *Tgfbr2*, the exon excised by Cre recombinase (Chytil et al., 2002), and found an ∼50% reduction in its expression in *Tnap*^{cre};*Tgfbr2*$^{fl/fl}$ compared to control (Fig. 3D). We confirmed this recombination efficiency by counting the number of TNAP/tdTomato double-positive cells over the total number of TNAP-positive cells in the *Tnap*^{cre};*Rosa26-tdTomato* mice (Fig. S3). Injection of control oil did not modify the expression of TNAP.

Journal of Cell Science (2019) 132, jcs234948. doi:10.1242/jcs.234948

Fig. 3. Deletion of *Tgfbr2* in TNAP-positive cells reduces Ang II-induced fibrosis in the heart. (A,B) Confocal images of sections from Sham- and Ang II-treated heart labelled for TNAP and TGF-βR2. Arrows indicates double-positive cell in the ventricle. High magnification images for separate channels shown are below (A′–B″′). (C) Schematic diagram of the experimental protocol. TAM, tamoxifen. (D) qRT-PCR was performed using *Tgfbr2*$^{fl/fl}$ and *Tnap*^{cre};*Tgfbr2*$^{fl/fl}$ heart ventricle extracts for the detection of *Tgfbr2* exon 4/5 (mean ±s.d., *n*=3). (E–L) Immunofluorescence imaging for tenascin C (E–G) and tenascin C and PECAM1 (I–K) on *Tnap*^{cre};*Tgfbr2*$^{fl/fl}$ mice without Ang II treatment, *Tgfbr2*$^{fl/fl}$ with Ang II treatment and *Tnap*^{cre};*Tgfbr2*$^{fl/fl}$ with Ang II treatment on heart ventricles sections. The percentage of interstitial (H) and vascular (L) fibrosis is shown for the three groups. The quantification was performed on six different sections for each sample (mean±s.d., *n*=7 and *n*=5 for each group, respectively). (M–Q) Hematoxylin/Eosin staining on heart sections from on *Tnap*^{cre};*Tgfbr2*$^{fl/fl}$ mice without Ang II treatment (M), *Tgfbr2*$^{fl/fl}$ with Ang II treatment (N) and *Tnap*^{cre};*Tgfbr2*$^{fl/fl}$ with Ang II treatment (O). (P) Heart to body weight ratio for the three groups. (Q) Quantification of cardiomyocyte diameter for the three groups (mean±s.d., *n*=4). (R–T) qRT-PCR for collagen 1a2, vimentin and *Sma* performed on on *Tnap*^{cre};*Tgfbr2*$^{fl/fl}$ mice without Ang II treatment, *Tgfbr2*$^{fl/fl}$ with Ang II treatment and *Tnap*^{cre};*Tgfbr2*$^{fl/fl}$ with Ang II treatment cDNA samples. Mean±s.d. normalized fold changes are shown (*n*=3). **P*<0.05, ***P*<0.01, ****P*<0.001, *****P*<0.0001; NS, not significant (two-tailed *t*-test). Scale bars: 20 µm.

We next quantified the area of fibrosis in *Tnap*^{cre};*Tgfbr2*$^{fl/fl}$ Sham-treated mice, *Tgfbr2*$^{fl/fl}$ mice treated with Ang II and *Tnap*^{cre};*Tgfbr2*$^{fl/fl}$ mice treated with Ang II. We found a strong reduction of interstitial and vascular fibrosis in the *Tnap*^{cre};*Tgfbr2*$^{fl/fl}$ Ang II treated mice in comparison with the *Tgfbr2*$^{fl/fl}$ mice treated with Ang II (Fig. 3E–L). This result was confirmed by Azan–Mallory staining and by immunofluorescence analysis, showing reduced expression of collagen 1a2 and MMP1 in *Tnap*^{cre};*Tgfbr2*$^{fl/fl}$ Ang II-treated mice in comparison with the *Tgfbr2*$^{fl/fl}$ treated with Ang II (Fig. S4a-i). We analysed cardiac hypertrophy in *Tnap*^{cre};*Tgfbr2*$^{fl/fl}$ mice treated with Ang II compared with the control by calculating the heart weight:body weight ratio and by measuring the area of cardiomyocytes, but we found no difference in cell size and in overall hypertrophy between the two groups (Fig. 3M–Q), indicating that the reduction of fibrosis is not accompanied by a reduction in hypertrophy. We next characterized the expression of fibrotic genes by qRT-PCR in the three sample groups and found a significant reduction in collagen 1a2 and vimentin expression in the *Tnap*^{cre};*Tgfbr2*$^{fl/fl}$ mice treated with Ang II compared with the controls (Fig. 3R,S), while *Sma* expression did not change (Fig. 3T). Moreover, also immunostaining with antibodies against collagen 1 and MMP1 showed a dramatic reduction of areas of fibrosis, as also confirmed by Azan–Mallory staining (Fig. S4). These data prove that TNAP is specifically expressed and upregulated in cells with active TGF-β signalling that underlie cardiac fibrosis. It is remarkable that a 50% reduction of expression in a minority of the cardiac cell population leads to a dramatic decrease in the level of fibrosis, suggesting a specific role of TNAP-positive cells in regulating fibrosis.

Since it has been previously shown that TNAP is upregulated in dystrophic muscles (Diaz-Manera et al., 2012), we asked whether the abrogation of TGF-β signalling in TNAP-positive cells in dystrophic mice could reduce skeletal muscle fibrosis. We took advantage of the α-sarcoglycan deficient (*Sgca*-null) mice, a model for limb-girdle muscular dystrophy 2D (Duclos et al., 1998), which develop severe fibrosis after 2 months of age. We generated a triple transgenic strain by crossing the *Sgca*-null mice with the *Tnap*^{cre};*Tgfbr2*$^{fl/fl}$ mouse. We injected 6–7-day-old pups with tamoxifen for 3 days and killed the mice when they were 2 months old (Fig. 4A). We measured the recombination efficiency of Cre recombinase by qRT-PCR and western blotting (Fig. 4B,C) and found it to be 50%. We next analysed the extent of fibrosis by measuring the percentage of tenascin C-positive regions and found a significant decrease in fibrosis in the tibialis anterior (TA), the gastrocnemius (GA) and the diaphragm (DIA) of the *Sgca*-null *Tnap*^{cre};*Tgfbr2*$^{fl/fl}$ mice compared with the *Sgca*-null controls (Fig. 4D–G). We analysed the level of collagen 1a2 by immunofluorescence (Fig. 4H) and the expression level of collagen 1a2, *Sma* and vimentin mRNA by qRT-PCR (Fig. 4I–K). We observed a significant reduction of their expression in the *Sgca*-null *Tnap*^{cre};*Tgfbr2*$^{fl/fl}$ mice compared with what was found in the *Sgca*-null controls. In order to reveal whether the reduction of fibrosis in the triple transgenic mice is sufficient to improve muscle strength and function, we measured muscle grip strength by placing mice on an upside down grid (Bonetto et al., 2015). Wild-type mice started to explore the environment and spent little time in the same location. In contrast *Sgca*-knockout mice spent 26% of the total time without moving, which importantly decreased to only 10% in the triple transgenic mice (Fig. 4L) (*n*=4 for each group). These data suggest that the reduction in fibrosis is associated with improved skeletal muscle function. Overall, the data so far demonstrate that cells that express TNAP in fibrotic cardiac and skeletal muscle are of pivotal significance in the TGF-β-dependent development of the pathology as inhibition of TGF-β signalling in these cells is sufficient to limit fibrosis.

TNAP inhibits SMAD2/3 phosphorylation and limits the expression of downstream fibrotic genes

Since we obtained similar results in cardiac and skeletal muscle models of fibrosis, we hypothesized that TNAP may have a role in the regulation of TGF-β signalling and that this role is conserved in both tissues. Being a phosphatase, TNAP could be involved in the dephosphorylation of phosphorylated (p-)SMAD2/3 and have thereby a regulatory role in the transcription of fibrotic genes. In order to test our hypothesis, we first verified whether TNAP and p-SMAD2/3 colocalize within the cell. We stained sections for TNAP and p-SMAD2/3 and saw that both of them partially colocalize in the peri-nuclear region (Fig. 5A). We confirmed their colocalization also *in vitro*. We transfected C2C12 skeletal myogenic cells with EYFP-SMAD2 and mCherry-TNAP plasmids and confirmed that the two proteins colocalize in intracellular vesicular compartments around the nucleus (Fig. 5B). Interestingly TNAP and SMAD2 colocalization was present in both Sham and Ang II treated mice (Fig. 5A). We found that TNAP not only colocalizes with SMAD2 but also physically interacts with it. We proved this by performing a proximity ligation assay (PLA) (Shah et al., 2017) (Fig. 5C) and co-immunoprecipitation for C2C12 cells transfected with Myc–TNAP (Fig. S5).

Our results show that endogenous SMAD2 interacts with Myc–TNAP. Notably, the TNAP–SMAD2 interaction not only occurs upon TGF-β stimulation, but also, at a lower level, under control conditions. In order to understand whether this interaction has a functional relevance on TGF-β signalling, we treated cardiac fibroblasts with TGF-β1 (5 ng/ml) and the specific TNAP inhibitor MLS-0038949 (Crowley et al., 2006) (200 nM) for 1 h and analysed SMAD2/3 phosphorylation by western blotting. The cells treated with TGF-β1 and TNAP inhibitor showed a significant increase in SMAD2/3 phosphorylation compared with cells treated with only TGF-β1 (Fig. 5D) (*n*=3 independent experiments), suggesting that the blockade of TNAP leads to enhanced TGF-β signalling. To provide further evidence for TNAP regulation of SMAD2/3 activity, we overexpressed plasmid encoding for Myc–TNAP in C2C12 skeletal muscle cells and stimulated the cells with TGF-β1 (5 ng/ml). We chose this cell line because it has no detectable

Journal of Cell Science (2019) 132, jcs234948. doi:10.1242/jcs.234948

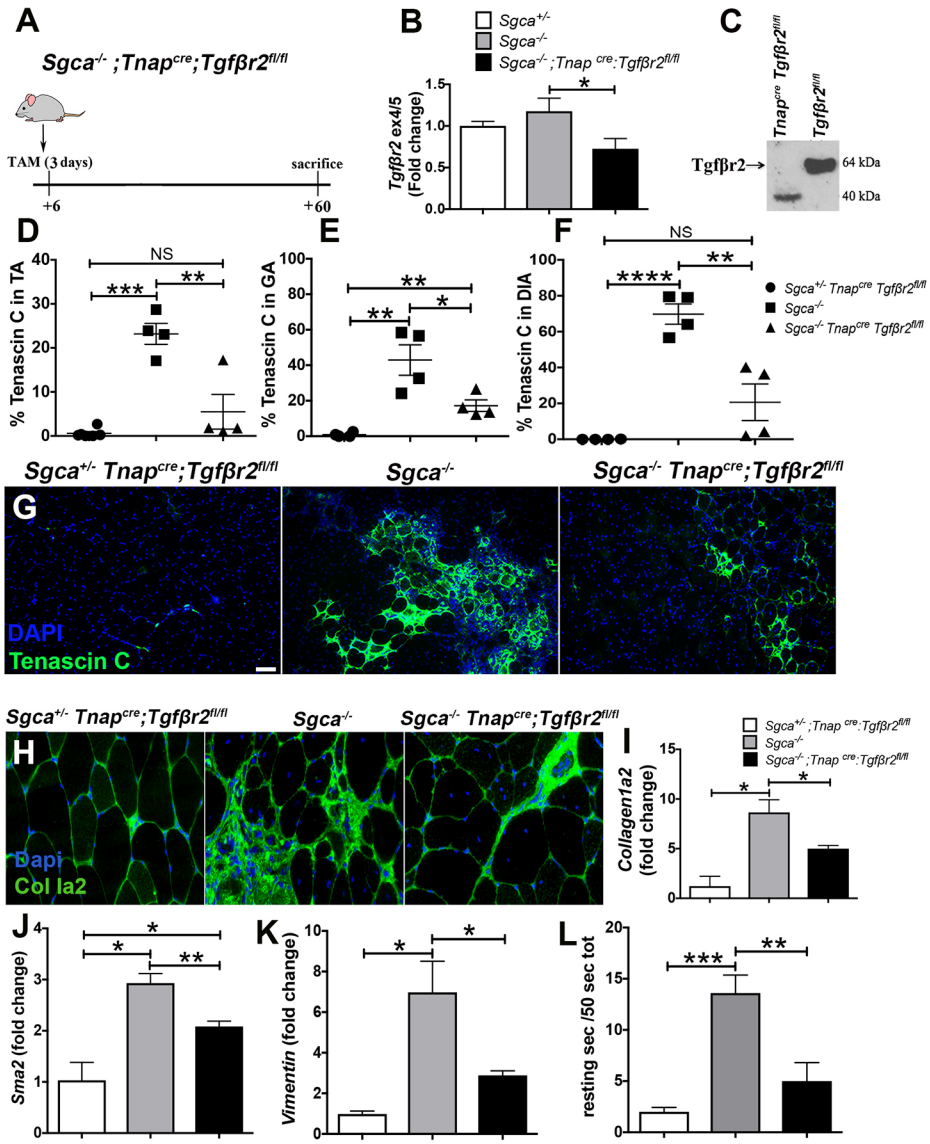

Fig. 4. Deletion of *Tgfbr2* in TNAP-positive cells reduces skeletal muscle fibrosis in *Sgca*$^{-/-}$ mice. (A) Schematic diagram of the experimental protocol. TAM, tamoxifen. (B) qRT-PCR on *Sgca*$^{+/-}$, *Sgca*$^{-/-}$ and *Sgca*$^{-/-}$ *Tnap*^{cre};*Tgfbr2*$^{fl/fl}$ tibialis anterior (TA) for the detection of the exon 4/5 of *Tgfbr2* (mean±s.d., *n*=3). (C) Western blot for Tgf-βRII on proteins extracts on *Tgfbr2*$^{fl/fl}$ and *Tnap*^{cre};*Tgfbr2*$^{fl/fl}$ mice. (D–F) Quantification of tenascin C-positive areas in *Sgca*$^{+/-}$, *Sgca*$^{-/-}$ and *Sgca*$^{-/-}$ *Tnap*^{cre};*Tgfbr2*$^{fl/fl}$ TA (D), Gastrocnemius (GA) (E) and Diaphragm (DIA) (F) muscles. The quantification was performed on six different sections for each sample. (G,H) Staining for tenascin C (G) and collagen 1a2 (H) on the TA of the three groups of mice. (I–K) qRT-PCR for collagen 1a2, *Sma* and vimentin, performed on *Sgca*$^{+/-}$, *Sgca*$^{-/-}$ and *Sgca*$^{-/-}$ *Tnap*^{cre};*Tgfbr2*$^{fl/fl}$ TA cDNA samples. Mean±s.d. normalized fold changes are shown (*n*=3). (L) Muscle grip strength test on *Sgca*$^{+/-}$, *Sgca*$^{-/-}$ and *Sgca*$^{-/-}$ *Tnap*^{cre};*Tgfbr2*$^{fl/fl}$ mice. The *y*-axis indicates the mean±s.d. of immobile time over a 50 s interval on an upside-down wireframe (*n*=4). **P*<0.05, ***P*<0.01, ****P*<0.001, *****P*<0.0001; NS, not significant. (two-tailed *t*-test). Scale bars: 50 µm.

TNAP expression (Fig. 5E). We verified that the plasmid was functional by performing a functional staining assay for AP in the C2C12 cells (Fig. 5F,G). Upon TGF-β1 stimulation, we detected a decrease in SMAD2/3 phosphorylation in Myc–TNAP overexpressing cells compared with the GFP control (Fig. 5H,I). Inhibition of SMAD2/3 phosphorylation was not dramatic because on average ∼20–30% of C2C12 cells are transiently transfected. Together, these data prove that TNAP is capable and in itself sufficient to limit SMAD2/3 phosphorylation. We next analysed the expression of fibrotic genes downstream p-SMAD2/3 by RT-qPCR and observed that expression of fibronectin 1, collagen 1a2 and tenascin C mRNAs were downregulated in Myc–TNAP-overexpressing cells compared with the control (Fig. 5J), indicating that TNAP-induced dephosphorylation of p-SMAD2/3 is sufficient to limit transcription of fibrotic genes. Taken together, these data indicate that TNAP regulates SMAD2/3 phosphorylation levels and is a direct attenuator of cellular pro-fibrotic signalling pathways.

DISCUSSION

Despite ever increasing understanding of the molecular processes that trigger fibrosis across different organs, there are only a few therapies available and most of them only indirectly target fibrotic processes (Rockey et al., 2015). TGF-β1 binding to the receptors on the plasma membrane leads to the phosphorylation of R-SMADs, their translocation into the nucleus and transcription of pro-fibrotic genes. Given the importance of TGF-β signalling and the phosphorylation of R-SMADs in fibrosis, the identification of phosphatases, able to switch off the TGF-β pathway, has been of interest for the past ten years since they could also be targets for anti-fibrotic drugs. Nevertheless, until now, only one phosphatase, PPM1A, has been identified (Lin et al., 2006). Here, we show that TNAP is able to dephosphorylate SMAD2/3 and consequently limit the transcription of pro-fibrotic genes.

An abundant literature exists on TNAP function in bone development and calcification (Byon et al., 2008; Millan, 2013); however, the role of TNAP in the heart has only been partly elucidated. TNAP overexpression has recently been associated with increased cardiac fibrosis and vascular calcification. Sheen et al. demonstrated that the induced expression of TNAP in vascular smooth muscle cells is sufficient to cause medial vascular calcification (Sheen et al., 2015). Similarly, Romanelli and colleagues showed that TNAP overexpression in vascular

Journal of Cell Science (2019) 132, jcs234948. doi:10.1242/jcs.234948

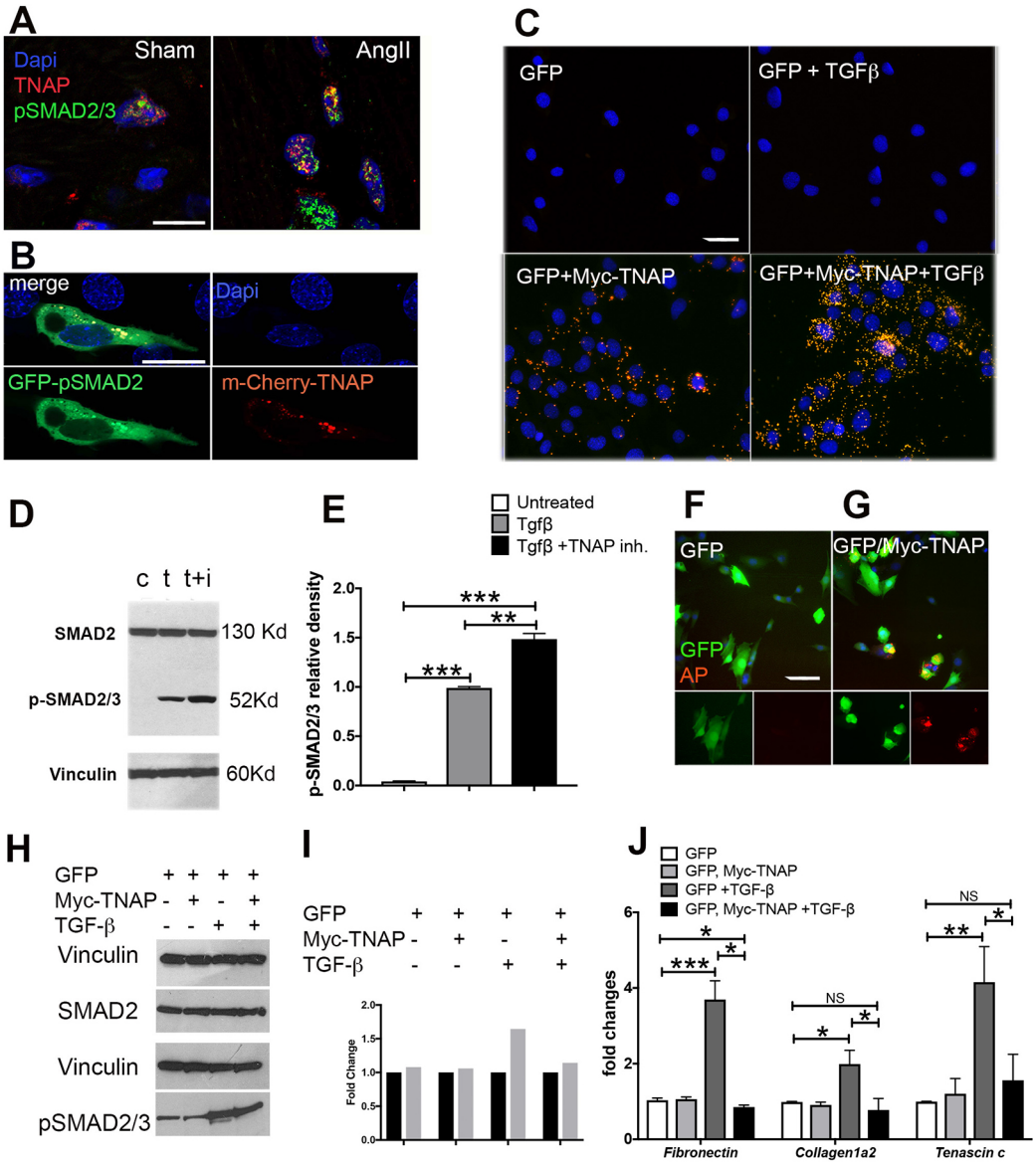

Fig. 5. TNAP regulates SMAD2/3-dependent TGF-β signalling. (A) Confocal images of TNAP and p-SMAD2/3 colocalization in Sham- and Ang II-treated heart sections. (B) Confocal images of intracellular colocalization of TNAP and SMAD2 in C2C12 cells transfected with EGFP–SMAD2 and mCherry–TNAP. (C) PLA analysis of Myc–TNAP interaction with endogenous SMAD2 in C2C12 cells that were left untreated or treated with 5 ng/ml of TGF-β1 for 3 h; GFP was used as transfection control (representative of *n*=3 independent experiments). (D) Western blot analysis for SMAD2 and p-SMAD2/3 on cell lysate from control primary cardiac fibroblasts treated with either 5 ng/ml of TGF-β1 (t) or 5 ng/ml of TGF-β1 and the TNAP inhibitor MLS-0038949 (200 nM) for 1 h (t+i); untreated cells were used as control (c). TNAP inhibition increases SMAD2/3 phosphorylation. (E) Densitometric analysis of the western blot analysis shown in D. (F,G) Immunofluorescence analysis for GFP and TNAP activity in C2C12 cells transfected with Myc–TNAP and GFP plasmids (G). C2C12 transfected only with GFP were used as control (F). (H) Western blot analysis for SMAD2 and p-SMAD2/3 on C2C12 cells transfected with Myc–TNAP and GFP plasmids, treated or untreated with 5 ng/ml TGF-β1 for 3 h; C2C12 cells transfected only with GFP plasmid were used as control. Myc–TNAP overexpression leads to reduced SMAD phosphorylation. (I) Densitometric analysis of the western blot shown in H. Grey bars, p-SMAD2/3; black bars, SMAD2. Each bar represents the value normalized to vinculin and plotted in relation to the level of SMAD2 in control, arbitrarily set at 1. (J) qRT-PCR for fibronectin, collagen 1a2 and tenascin C performed on cDNA samples from C2C12 transfected with Myc–TNAP and GFP plasmids treated with either 5 ng/ml of TGF-β1 for 3 h or untreated; C2C12 cells transfected only with GFP were used as control. Normalized fold changes (mean±s.d.) are shown (*n*=3 independent experiments). Scale bars: 20 µm. **P*<0.05, ***P*<0.01, ****P*<0.001; NS, not significant (two-tailed *t*-test).

endothelium in mice leads to arterial calcification and subsequent coronary atherosclerosis (Romanelli et al., 2017). These studies described the effects of sustained TNAP overexpression, but the role of TNAP under physiological levels of expression has not been addressed. Indeed, it is counterintuitive that tissues where calcification is exclusively pathological have maintained TNAP expression during evolution. This suggests that TNAP may also play beneficial roles in striated muscle that is eventually overridden by sustained fibrotic stimuli; however, this role has thus far remained unknown. Here, we analysed two different models of fibrosis: rapid-onset cardiac fibrosis induced by the hypertensive molecule Ang II, and chronic skeletal muscle fibrosis in the *Sgca*-null mice. We confirm earlier evidence showing that TNAP is upregulated in tissue fibrosis (Herencia et al., 2015; Gan et al., 2014), but also show here that the number of cells expressing TNAP increases in both heart and skeletal muscle. Furthermore, as the abrogation of TGF-β

Journal of Cell Science (2019) 132, jcs234948. doi:10.1242/jcs.234948

signalling in TNAP-positive cells dramatically reduces vascular and interstitial fibrosis, we can conclude that TNAP is actively expressed in cells driving tissue fibrosis. Since in the heart, not only interstitial and perivascular cells, but also endothelial cells and cardiomyocytes participate in the process (though likely to a minor extent), it is interesting to note that TNAP has a similar pattern of expression, being more abundant in interstitial and perivascular cells but also present in the other cell types of the heart.

TGF-β signalling relies on trafficking of activated phosphorylated R-SMAD proteins from the plasma membrane to the nucleus (Chen, 2009; Hough et al., 2012; Nakao et al., 1997). SMAD2/3 inactivation during this process would enable a cell to rapidly limit the expression of pro-fibrotic genes even in the presence of TGF-β secreted in the inflammatory tissue environment. Here, we show that TNAP inhibition enhances SMAD2/3 phosphorylation whereas TNAP overexpression has the opposite effect. We demonstrate that TNAP interacts with SMAD2. Our data collectively prove that TNAP is an efficient inhibitor of SMAD2/3 and limits SMAD-dependent transcription of pro-fibrotic genes. Intriguingly, TNAP interacts with SMAD2 even in cells that are not exposed to TGF-β1. These results demonstrate that TNAP likely has a housekeeping function during normal tissue growth and homeostasis, which explains its basal level expression in cardiac and skeletal muscle. In addition to the molecular mechanism described here, TNAP may also indirectly affect the activity of numerous phosphorylation-dependent pathways as this enzyme is known to regulate the level of cytoplasmic inorganic phosphate (Pi) (Hessle et al., 2002).

In conclusion, we show here that the ubiquitously expressed TNAP is an essential regulator of SMAD2/3-dependent TGF-β signalling in physiological conditions and in tissue fibrosis. These results provide a novel insight into the mechanisms that control the expression of extracellular matrix genes and may lead to the development of novel therapies for fibrosis.

MATERIALS AND METHODS

Animals

Mice were maintained in pathogen-free conditions at Manchester University animal facility and fed standard rodent diet. Animal studies were performed according to the United Kingdom Animals (Scientific Procedures) Act 1986 and approved by the University of Manchester Ethics Committee. Angiotensin experiments were approved under Home Office license no. 40/3625 and no. P3A97F3D1. All the other experiments were approved under licence no.707435. *Sgca*-null mice (Duclos et al., 1998), $Tnap^{cre}$ mice (Dellavalle et al., 2011) and $Tgfbr2^{flox/flox}$ (Chytil et al., 2002) mice were backcrossed onto C57BL/6 mice (Charles River Laboratories Inc., Wilmington, MA) and were genotyped as previously described (Dellavalle et al., 2011). *Rosa26NZG* mice were obtained from the Jackson laboratory. Mice were culled by administration of isoflurane and consequent cervical dislocation at appropriate time points. Hearts and muscles were collected in ice-cold PBS and then embedded in glue or OCT inclusion medium. Samples were stored at −80°C before processing.

Osmotic minipump infusion of angiotensin II and tamoxifen administration

In order to induce cardiac hypertrophy, angiotensin II (Sigma-Aldrich, St. Louis, MO, USA, Cat. No. A9525) (2.8 mg/kg of body weight/day) or vehicle (ddH_2O) was administrated to 10-week-old wild type (wt) and transgenic male mice via osmotic mini-pumps (1002, Alzet, Cupertino, CA) implanted subcutaneously. Briefly, the mice were anaesthetized with isoflurane (5% induction; 2–3% maintenance) in oxygen, using a small nose cone attached to a modified Bane circuit. The skin on the dorsal surface of the animal was shaved with a clipper, and sterile scissors were used to make a 0.5 cm horizontal incision. Subcutaneous tissue was spread using a haemostat to create a pocket in which the minipump was inserted. The incision was closed with absorbable suture (5-0 Maxon). After the surgery the mice received 0.1 mg/kg of body weight of buprenorphine and were allowed to recover before being returned to the home cage. Hearts were isolated and analysed for cardiac hypertrophy following 14 days of Ang II infusion. In order to induce the expression of the Cre recombinase in the null $Tnap^{cre}$ $Tgfbr2^{fl/fl}$ and $Sgca^{-/-}$ $Tnap^{cre}$;$Tgfbr2^{fl/fl}$ mice, tamoxifen (Sigma-Aldrich, Cat. No. T5648) was dissolved in corn oil (Sigma-Aldrich, Cat. No. C8267) and injected at the following concentrations and time points: 0.3 mg/mouse in 6-day-old pups once a day for 3 consecutive days, and 3 mg/mouse in 10-week-old mice once a day for 5 consecutive days.

Grip test

The four limb-hanging test (also known as Kondziella's inverted screen test) (Bonetto et al., 2015) represents a method to assess muscle strength using all four limbs and to determine the general condition over time. In this study, we modified this method to improve its reproducibility. Briefly, we placed the mice upside down on a grid (50 cm×30 cm) and we counted the number of seconds in which the mice were not moving on the grid, over a total period of 50 s each mice. We calculated the resting time on the grid as the average of three different tests for each mouse, and we analysed four mice per each group.

PLA and immunofluorescence

PLA was performed according to the manufacturer's instructions using the Duolink In Situ Orange Kit Goat/Rabbit (Sigma-Aldrich, Cat. No. DUO92106). Immunofluorescence was performed as previously described (Arn et al., 2014). Briefly sections (5 µm) were fixed in 4% paraformaldehyde (Sigma-Aldrich, Cat. No. P6148) in PBS, pH 7.2 for 20 min; then washed three times, 5 min each, in PBS and the blockage of non-specific binding was undertaken with blocking buffer [1× PBS, 10% fetal bovine serum (FBS), 1 mg/ml bovine serum albumin (BSA), 0.1% Triton X-100], for 1 h at room temperature. For all steps, slides were kept in humidified chambers. For the TNAP staining, the sections were additionally fixed with methanol-acetone for 10 min. Antibodies were diluted in blocking buffer and incubated at +4°C overnight as suggested by manufacturer's instructions. The following day, sections were rinsed in PBS three times for 5 min each time, and fluorescent secondary antibodies, (Alexa Fluor conjugated, Thermo Fisher Scientific) diluted in blocking buffer were applied according to the manufacturer's instructions. Slides were washed three times in PBS for 5 min each time and incubated in DAPI (Sigma-Aldrich, Cat. No. 10236276001) for nuclei counterstaining. The following antibodies were used: goat anti-TNAP (Santa Cruz Biotechnology, Dallas, TX, Cat. No. c-23430), 1:100; rabbit anti-TNAP (Abgent, Suzhou city, China, Cat. No. AP1474C), 1:100; rat anti-PECAM (Dev. Studies Hybridoma Bank), 1:3; rabbit anti-laminin (Santa Cruz Biotechnology, Cat. No. sc-17810), 1:100; chicken anti-GFP (Abcam, Cambridge, UK, Cat. No. ab13970), 1:500; rabbit anti-collagen 1a2 (Merck Millipore, Billerica, MA, Cat. No. AB 745), 1:75; rabbit anti-tenascin C (Merck Millipore, Cat. No. AB19013), 1:150; chicken anti-vimentin (Novus biologicals, Littleton, CO, Cat. No. NB300-223) 1:300; rabbit anti -TGF-βR2 (Novus Biologicals, Cat. No. NB100-91994), 1:100; rabbit anti-SMAD2 (Cell Signalling, Danvers, MA, Cat. No. D43B4), 1:100; rabbit anti-pSMAD2/3 (Cell Signalling, Cat. No. D27F4), 1:100; and rabbit anti-Ki67 (Abcam, Cat. No. ab15580), 1:200. Appropriate fluorophore-conjugated secondary antibodies (Alexa Fluor 488, 594 and 647, Molecular Probes) were applied. Nuclei were visualized using DAPI. For the detection of TNAP activity, the Red Alkaline Phosphatase (Red AP) substrate kit (VECTOR Laboratories, Peterborough, UK, SK-5100) was used according to manufacturer's instructions. Light (Zeiss Axio Imager M2, with 5×, 10× and 20× objectives) and confocal (Leica, SP5 with ×40 and ×63 objectives) microscopy was performed to analyse tissue and cell staining. For confocal imaging, pictures were acquired at 1× line average and 3× frame average on a single confocal plane. Analysis was performed by using Zeiss ZEN 2 software and Adobe Photoshop CS5 Version 12.0×64 software. Quantification of tenascin C-positive regions in hearts and skeletal muscles was performed by using ImageJ 2.0.0-rc-9.

Cell culture

C2C12 cells from European Collection of Authenticated Cell Cultures, Public Health England (Porton Down, UK) were cultured in DMEM (Gibco, Thermo Fisher Scientific, Waltham, MA), supplemented with 1% L-glutamine, 10% fetal bovine serum (FBS), 1% penicillin-streptomycin (Thermo Fisher Scientific, Cat. No. 15140122). Cells were transfected with Lipofectamine 2000 (Thermo Fisher Scientific, Cat. No. 11668027) according to manufacturer's instructions. The following plasmids were used for transfection: pEGFP-N1 (Clontech, Cat. No. 6085-1), pCDNA3.1 N-Myc-TNAP and pCDNA3-mCherry TNAP. In detail, the Smad2/TNAP ORF was RT-PCR amplified from mouse cDNA. PCR products were inserted into EcoRI/XhoI site of the EYFP/mCherry/myc-pcDNA3 vectors.

Cardiac fibroblasts were obtained from neonatal and adult C57Bl/6 mice. Mice were killed by cervical dislocation and their hearts were rapidly removed. The hearts were then mashed with scalpels and digested with 10 ml collagenase solution [120 mg collagenase A (Roche, Cat. No. 10 103 578 001) and 12 mg protease (Sigma-Aldrich, Cat. No. 10165921001) dissolved in 80 ml PBS solution] at 37°C for 15 min, for five times. Cells were collected after each digestion and the collagenase was deactivated by addition of 50% FBS. The fibroblasts were centrifuged for 5 min at 220 ***g***. The cell pellet was resuspended in 10ml ACF medium (80% DMEM, 20% FBS, 1% penicillin/streptomycin and 1% non-essential amino acids). Fibroblasts were then plated in 10 ml delta-NUNC tissue culture plates (Thermo Fisher Scientific, Cat. No. 150318) overnight. The next day, the medium was removed and replaced with 10 ml ACF medium. C2C12 and cardiac fibroblasts were serum starved for 24 h before adding medium containing 5 ng/ml recombinant TGF-β1 for 2 days (R&D Systems, Minneapolis, MN, Cat. No. 7666-MB-005).

Western blot and immunoprecipitation

Hearts and skeletal muscles from wild-type, *Tnap*^{cre};*Tgfbr2*$^{fl/fl}$ and α-sarcoglycan-null *Tnap*^{cre};*Tgfbr2*$^{fl/fl}$ and controls were homogenized with the homogenizer SHM1 (Stuart Equipment Stone, Staffordshire, UK, Cat. No. 1171631) in RIPA lysis buffer [50 mM Tris-HCl pH 8.0, 150 mM NaCl, 1% NP-40, 0.5% sodium deoxycholate, 0.1% SDS, supplemented with phosphatase and protease inhibitor cocktail (Sigma-Aldrich, Cat. No. PCC 1010)]. Cold lysis buffer (RIPA) was added into the wells after removing the media and washing the cells with PBS. The cells were scraped into sterile, pre-cooled tubes. The samples were incubated (with rotation) for 30–60 min at 4°C. Soluble proteins were quantified with a Bradford Protein Assay Kit (Bio-Rad, Cat. No. 5000006). 50 µg of protein extract was subjected to SDS-PAGE and subsequently blotted on to a nitrocellulose membrane. For immunoprecipitation experiments, C2C12 cells were collected in lysis buffer (50 mM Tris-HCl pH 7.8, 150 mM NaCl, 1 mM $CaCl_2$ and 1% Triton X-100) supplemented with protease inhibitor cocktail (Sigma-Aldrich, Cat. No. P8340). 1 mg/ml of pre-cleared lysates were incubated with anti-Smad2 (Cell Signalling, Cat. No. D43B4) at a dilution of 1:50 or the negative control rabbit IgG in lysis buffer with rotation overnight at +4°C. The samples were then incubated with protein A magnetic beads (Merck Millipore, Cat. No. LSKMAGA10) for 1 h at +4°C (with rotation) and the immunocomplexes were detected by western blotting. The following primary antibodies were used: goat anti-Myc (Abcam, Cat. No. ab9132), 1:1000; rabbit anti-TGF-βRII (Novus Biologicals, Cat. No. NB100- 91994), 1:500; mouse anti-vinculin (Santa Cruz Biotechnology, Cat. No. H300), 1:6000; rabbit anti-SMAD2 (Cell Signalling, Cat. No. D43B4), 1:1000; rabbit anti-pSMAD2/3 (Cell Signalling, Cat. No. D27F4), 1:1000. Secondary antibodies (Dako Donkey anti-goat P0449; Dako Goat anti-rabbit P0448) were incubated for 1 h at room temperarure, and signals were revealed using Millipore ECL kit (Cat. No. WBKLS0500). For quantitative measurement, blots were analysed with ImageJ 2.0.0-rc-9, normalizing band intensities to vinculin levels.

Real-time and standard RT-PCR

Total RNA from heart, skeletal muscle and cells was extracted by homogenizing the samples in Trizol (Thermo Fisher Scientific, Cat. No. 15596018) reagent following the standard manufacturer's procedure. Chloroform was added to the samples, which were incubated for 15 min at room temperature and then centrifuged at 12,000 ***g*** for 15 min. The aqueous layer was mixed with isopropanol, incubated for 10 min and centrifuged for 10 min at 12,000 ***g***. 75% of ethanol was added and the samples were centrifuged at 12,000 ***g*** for 15 min. After the elimination of ethanol, the RNA was dissolved in 50 µl of water. DNase (Thermo Fisher Scientific, Cat. No. 18068015) digestion was done on all the samples. RNA was quantified with a Nanodrop 2000 and equalized to give the same concentration before cDNA synthesis. cDNA synthesis was performed using ThermoScript RT-PCR System (Thermo Fisher Scientific, Cat. No. K1622) according to the manufacturer's instructions in final volume of 20 µl. qRT-PCR was carried out using FastStart Essential DNA Master Mix (Cat. No. 06402712001; Roche diagnostics GmbH, Mannheim, Germany). qRT-PCR was performed in five biological replicates, using a standard dilution series on every plate. Samples were normalized to the values for the housekeeping genes *Gapdh* and *Rlp19* with the following primers: *Gapdh* F, 5′-AGGTCGGTGTGAACGGATT-3′, *Gapdh* R, 5′-TGTAGACCATGTAGTTGAG-3′ and *Rpl19* F, 5′-ATGAGTATGCTCAGGCTACAGA-3′ and *Rpl19* R, 5′-GCATTGGCGATTTCATTGGTC-3′. Specific primers were used for gene expression analysis were: tenascin C, F, 5′-ACGGCTACCACAGAAGCTG-3′; R, 5′-ATGGCTGTTGTTGCTATGGCA-3′; Fibronectin 1, F, 5′-TTCAAGTGTGATCCCCATGAAG-3′; R, 5′-CAGGTCTACGGCAGTTGTCA-3′; vimentin, F, 5′-CGGCTGCGAGAGAAATTGC-3′; R, 5′-CCACTTTCCGTTCAAGGTCAAG-3′; *Tgfbr2* exon4/5, F, 5′-GACCTCAAGAGCTCTAACATCC-3′; R, 5′-CTAGAACTTCCGGGGCCATG-3′; *Tgfbr2*, F, 5′-CCGCTGCATATCGTCCTGTG-3′; R, 5′-AGTGGATGGATGGTCCTATTACA-3′; *Sma*, F, 5′-CCCAGACATCAGGGAGTAATGG-3′; R, 5′-TCTATCGGATACTTCAGCGTCA-3′; *Col1a2*, F, 5′-GGAGAGAGGAGTCGTTGGAC-3′; R, 5′-GTTCACCCTTCACACCCTGT-3′; *Gapdh*, F, 5′-TTCACCATGGAGAAGGC-3′; R, 5′-GGCATGGACTGTGGTCATGA-3′; *Tnap*, F, 5′-GTGGATACACCCCCCGGGGC-3′; R, 5′-GGTCAACCTTCCCCCCAATGCA-3′; *Alpi*, F, 5′-ATGATGCCAACCGAAACCC C; R, 5′-GCGTGTCCTTCTCATTGGTAA-3′; *Alpg*, F, 5′-GAGCGTCATCCCAGTGGAG-3′; R, 5′-GGTAGCGGTTACTGTAGACACC-3′.

Statistics

Data are expressed as the mean±s.d. or mean±s.e.m. of independent experiments. Comparisons were made using an unpaired *t*-test. Statistical tests were carried out using PRISM6.0e (GraphPad Software, La Jolla, CA). $P<0.05$ was considered statistically significant.

Competing interests

The authors declare no competing or financial interests.

Author contributions

Conceptualization: B.A., F.G., J.C.M., E.J.C., G.C.; Methodology: B.A., F.G., U.R., B.M.A., T.M., A.A., L.B., S.P.; Validation: F.G., U.R., B.M.A.; Formal analysis: B.A., B.M.A.; Investigation: B.A., F.G., U.R., T.M., A.A., L.B., S.P., G.C.; Resources: T.M.; Data curation: U.R., B.M.A., A.A., L.B., S.P., J.C.M., G.C.; Writing - original draft: F.G., J.C.M., E.J.C., G.C.; Writing - review & editing: B.A., J.C.M., E.J.C., G.C.; Supervision: J.C.M., E.J.C.; Funding acquisition: J.C.M., E.J.C., G.C.

Funding

B.A. was supported by British Heart Foundation (PG/14/1/30549). U.R. was supported by an Biotechnology and Biological Sciences Research Council Anniversary Future Leader Fellowship (BB/M013170/1). J.C.M. and T.M. were supported by the Canadian Institutes of Health Research (CIHR). E.J.C. was supported by British Heart Foundation (PG/14/1/30549). G.C. was supported by British Heart Foundation (PG/14/1/30549), the Medical Research Council (MR/P016006/1), Duchenne Parent Project (Italy), the Great Ormond Street Hospital Charity - Sparks Charity (V4618).

Supplementary information

Supplementary information available online at
http://jcs.biologists.org/lookup/doi/10.1242/jcs.234948.supplemental

References

Alnaqeeb, M. A., Al Zaid, N. S. and Goldspink, G. (1984). Connective tissue changes and physical properties of developing and ageing skeletal muscle. *J. Anat.* **139**, 677-689.

Arnò, B., Grassivaro, F., Rossi, C., Bergamaschi, A., Castiglioni, V., Furlan, R., Greter, M., Favaro, R., Comi, G., Becher, B. et al. (2014). Neural progenitor cells orchestrate microglia migration and positioning into the developing cortex. *Nat. Commun.* **5**, 5611. doi:10.1038/ncomms6611

Berk, B. C., Fujiwara, K. and Lehoux, S. (2007). ECM remodeling in hypertensive heart disease. *J. Clin. Invest.* **117**, 568-575. doi:10.1172/JCI31044
Bernaba, B. N., Chan, J. B., Lai, C. K. and Fishbein, M. C. (2010). Pathology of late-onset anthracycline cardiomyopathy. *Cardiovasc. Pathol.* **19**, 308-311. doi:10.1016/j.carpath.2009.07.004
Bonetto, A., Andersson, D. C. and Waning, D. L. (2015). Assessment of muscle mass and strength in mice. *Bonekey Rep.* **4**, 732. doi:10.1038/bonekey.2015.101
Bruce, D. L. and Sapkota, G. P. (2012). Phosphatases in SMAD regulation. *FEBS Lett.* **586**, 1897-1905. doi:10.1016/j.febslet.2012.02.001
Byon, C. H., Javed, A., Dai, Q., Kappes, J. C., Clemens, T. L., Darley-Usmar, V. M., McDonald, J. M. and Chen, Y. (2008). Oxidative stress induces vascular calcification through modulation of the osteogenic transcription factor Runx2 by AKT signaling. *J. Biol. Chem.* **283**, 15319-15327. doi:10.1074/jbc.M800021200
Chen, Y.-G. (2009). Endocytic regulation of TGF-beta signaling. *Cell Res.* **19**, 58-70. doi:10.1038/cr.2008.315
Chytil, A., Magnuson, M. A., Wright, C. V. E. and Moses, H. L. (2002). Conditional inactivation of the TGF-beta type II receptor using Cre:Lox. *Genesis* **32**, 73-75. doi:10.1002/gene.10046
Clarke, D. C., Brown, M. L., Erickson, R. A., Shi, Y. and Liu, X. (2009). Transforming growth factor beta depletion is the primary determinant of Smad signaling kinetics. *Mol. Cell. Biol.* **29**, 2443-2455. doi:10.1128/MCB.01443-08
Crowley, S. D., Gurley, S. B., Herrera, M. J., Ruiz, P., Griffiths, R., Kumar, A. P., Kim, H.-S., Smithies, O., Le, T. H. and Coffman, T. M. (2006). Angiotensin II causes hypertension and cardiac hypertrophy through its receptors in the kidney. *Proc. Natl. Acad. Sci. USA* **103**, 17985-17990. doi:10.1073/pnas.0605545103
Dellavalle, A., Sampaolesi, M., Tonlorenzi, R., Tagliafico, E., Sacchetti, B., Perani, L., Innocenzi, A., Galvez, B. G., Messina, G., Morosetti, R. et al. (2007). Pericytes of human skeletal muscle are myogenic precursors distinct from satellite cells. *Nat. Cell Biol.* **9**, 255-267. doi:10.1038/ncb1542
Dellavalle, A., Maroli, G., Covarello, D., Azzoni, E., Innocenzi, A., Perani, L., Antonini, S., Sambasivan, R., Brunelli, S., Tajbakhsh, S. et al. (2011). Pericytes resident in postnatal skeletal muscle differentiate into muscle fibres and generate satellite cells. *Nat. Commun.* **2**, 499. doi:10.1038/ncomms1508
Díaz-Manera, J., Gallardo, E., de Luna, N., Navas, M., Soria, L., Garibaldi, M., Rojas-García, R., Tonlorenzi, R., Cossu, G. and Illa, I. (2012). The increase of pericyte population in human neuromuscular disorders supports their role in muscle regeneration in vivo. *J. Pathol.* **228**, 544-553. doi:10.1002/path.4083
Di Guglielmo, G. M., Le Roy, C., Goodfellow, A. F. and Wrana, J. L. (2003). Distinct endocytic pathways regulate TGF-beta receptor signalling and turnover. *Nat. Cell Biol.* **5**, 410-421. doi:10.1038/ncb975
Duclos, F., Moore, S. A., Venzke, D. P., Hrstka, R. S., Crosbie, R. H., Durbeej, M., Lebakken, C. S., Ettinger, A. J., van der Meulen, J., Holt, K. H. et al. (1998). Progressive Muscular Dystrophy in a-Sarcoglycan–deficient Mice. *J. Cell Biol.* **142**, 1461-1468. doi:10.1083/jcb.142.6.1461
Dupont, S., Zacchigna, L., Cordenonsi, M., Soligo, S., Adorno, M., Rugge, M. and Piccolo, S. (2005). Germ-layer specification and control of cell growth by Ectodermin, a Smad4 ubiquitin ligase. *Cell* **121**, 87-99. doi:10.1016/j.cell.2005.01.033
Dupont, S., Inui, M. and Newfeld, S. J. (2012). Regulation of TGF-beta signal transduction by mono- and deubiquitylation of Smads. *FEBS Lett.* **586**, 1913-1920. doi:10.1016/j.febslet.2012.03.037
Episkopou, V., Arkell, R., Timmons, P. M., Walsh, J. J., Andrew, R. L. and Swan, D. (2001). Induction of the mammalian node requires Arkadia function in the extraembryonic lineages. *Nature* **410**, 825-830. doi:10.1038/35071095
Frangogiannis, N. G. (2012). Regulation of the inflammatory response in cardiac repair. *Circ. Res.* **110**, 159-173. doi:10.1161/CIRCRESAHA.111.243162
Gan, X. T., Taniai, S., Zhao, G., Huang, C. X., Velenosi, T. J., Xue, J., Urquhart, B. L. and Karmazyn, M. (2014). CD73-TNAP crosstalk regulates the hypertrophic response and cardiomyocyte calcification due to alpha1 adrenoceptor activation. *Mol. Cell. Biochem.* **394**, 237-246. doi:10.1007/s11010-014-2100-9
Grönroos, E., Hellman, U., Heldin, C.-H. and Ericsson, J. (2002). Control of Smad7 stability by competition between acetylation and ubiquitination. *Mol. Cell* **10**, 483-493. doi:10.1016/S1097-2765(02)00639-1
Heldin, C.-H., Miyazono, K. and ten Dijke, P. (1997). TGF-beta signalling from cell membrane to nucleus through SMAD proteins. *Nature* **390**, 465-471. doi:10.1038/37284
Herencia, C., Rodríguez-Ortiz, M. E., Muñoz-Castañeda, J. R., Martinez-Moreno, J. M., Canalejo, R., Montes de Oca, A., Diaz-Tocados, J. M., Peralbo-Santaella, E., Marin, C., Canalejo, A. et al. (2015). Angiotensin II prevents calcification in vascular smooth muscle cells by enhancing magnesium influx. *Eur. J. Clin. Investig.* **45**, 1129-1144. doi:10.1111/eci.12517
Hessle, L., Johnson, K. A., Anderson, H. C., Narisawa, S., Sali, A., Goding, J. W., Terkeltaub, R. and Millan, J. L. (2002). Tissue-nonspecific alkaline phosphatase and plasma cell membrane glycoprotein-1 are central antagonistic regulators of bone mineralization. *Proc. Natl. Acad. Sci. USA* **99**, 9445-9449. doi:10.1073/pnas.142063399
Hough, C., Radu, M. and Doré, J. J. E. (2012). Tgf-beta induced Erk phosphorylation of smad linker region regulates smad signaling. *PLoS ONE* **7**, e42513. doi:10.1371/journal.pone.0042513
Kania, G., Blyszczuk, P. and Eriksson, U. (2009). Mechanisms of cardiac fibrosis in inflammatory heart disease. *Trends Cardiovasc. Med.* **19**, 247-252. doi:10.1016/j.tcm.2010.02.005
Kretzschmar, M., Doody, J. and Massague, J. (1997). Opposing BMP and EGF signalling pathways converge on the TGF-beta family mediator Smad1. *Nature* **389**, 618-622. doi:10.1038/39348
Lin, X., Liang, M. and Feng, X.-H. (2000). Smurf2 is a ubiquitin E3 ligase mediating proteasome-dependent degradation of Smad2 in transforming growth factor-beta signaling. *J. Biol. Chem.* **275**, 36818-36822. doi:10.1074/jbc.C000580200
Lin, X., Duan, X., Liang, Y.-Y., Su, Y., Wrighton, K. H., Long, J., Hu, M., Davis, C. M., Wang, J., Brunicardi, F. C. et al. (2006). PPM1A functions as a Smad phosphatase to terminate TGFbeta signaling. *Cell* **125**, 915-928. doi:10.1016/j.cell.2006.03.044
Lönn, P., van der Heide, L. P., Dahl, M., Hellman, U., Heldin, C.-H. and Moustakas, A. (2010). PARP-1 attenuates Smad-mediated transcription. *Mol. Cell* **40**, 521-532. doi:10.1016/j.molcel.2010.10.029
Miles, W. O., Jaffray, E., Campbell, S. G., Takeda, S., Bayston, L. J., Basu, S. P., Li, M., Raftery, L. A., Ashe, M. P., Hay, R. T. et al. (2008). Medea SUMOylation restricts the signaling range of the Dpp morphogen in the Drosophila embryo. *Genes Dev.* **22**, 2578-2590. doi:10.1101/gad.494808
Millan, J. L. (2013). The role of phosphatases in the initiation of skeletal mineralization. *Calcif. Tissue Int.* **93**, 299-306. doi:10.1007/s00223-012-9672-8
Minasi, M. G., Riminucci, M., De Angelis, L., Borello, U., Berarducci, B., Innocenzi, A., Caprioli, A., Sirabella, D., Baiocchi, M., De Maria, R. et al. (2002). The meso-angioblast: a multipotent, self-renewing cell that originates from the dorsal aorta and differentiates into most mesodermal tissues. *Development* **129**, 2773-2783. doi:10.3410/f.1007112.94856
Mornet, E., Stura, E., Lia-Baldini, A.-S., Stigbrand, T., Ménez, A. and Le Du, M.-H. (2001). Structural evidence for a functional role of human tissue nonspecific alkaline phosphatase in bone mineralization. *J. Biol. Chem.* **276**, 31171-31178. doi:10.1074/jbc.M102788200
Nakao, A., Imamura, T., Souchelnytskyi, S., Kawabata, M., Ishisaki, A., Oeda, E., Tamaki, K., Hanai, J., Heldin, C. H., Miyazono, K. et al. (1997). TGF-beta receptor-mediated signalling through Smad2, Smad3 and Smad4. *EMBO J.* **16**, 5353-5362. doi:10.1101/gad.494808
Rockey, D. C., Bell, P. D. and Hill, J. A. (2015). Fibrosis–a common pathway to organ injury and failure. *N Engl. J. Med.* **372**, 1138-1149. doi:10.1056/NEJMra1300575
Romanelli, F., Corbo, A., Salehi, M., Yadav, M. C., Salman, S., Petrosian, D., Rashidbaigi, O. J., Chait, J., Kuruvilla, J., Plummer, M. et al. (2017). Overexpression of tissue-nonspecific alkaline phosphatase (TNAP) in endothelial cells accelerates coronary artery disease in a mouse model of familial hypercholesterolemia. *PLoS ONE* **12**, e0186426. doi:10.1371/journal.pone.0186426
Serrano, A. L. and Muñoz-Cánoves, P. (2017). Fibrosis development in early-onset muscular dystrophies: Mechanisms and translational implications. *Semin. Cell Dev. Biol.* **64**, 181-190. doi:10.1016/j.semcdb.2016.09.013
Shah, A. V., Birdsey, G. M., Peghaire, C., Pitulescu, M. E., Dufton, N. P., Yang, Y., Weinberg, I., Osuna Almagro, L., Payne, L., Mason, J. C. et al. (2017). The endothelial transcription factor ERG mediates Angiopoietin-1-dependent control of Notch signalling and vascular stability. *Nat. Commun.* **8**, 16002. doi:10.1038/ncomms16002
Sheen, C. R., Kuss, P., Narisawa, S., Yadav, M. C., Nigro, J., Wang, W., Chhea, T. N., Sergienko, E. A., Kapoor, K., Jackson, M. R. et al. (2015). Pathophysiological role of vascular smooth muscle alkaline phosphatase in medial artery calcification. *J. Bone Miner. Res.* **30**, 824-836. doi:10.1002/jbmr.2420
Tedesco, F. S. and Cossu, G. (2012). Stem cell therapies for muscle disorders. *Curr. Opin. Neurol.* **25**, 597-603. doi:10.1097/WCO.0b013e328357f288
Ueha, S., Shand, F. H. W. and Matsushima, K. (2012). Cellular and molecular mechanisms of chronic inflammation-associated organ fibrosis. *Front. Immunol.* **3**, 71. doi:10.3389/fimmu.2012.00071
Wood, L. K., Kayupov, E., Gumucio, J. P., Mendias, C. L., Claflin, D. R. and Brooks, S. V. (2014). Intrinsic stiffness of extracellular matrix increases with age in skeletal muscles of mice. *J. Appl. Physiol.* **117**, 363-369. doi:10.1152/japplphysiol.00256.2014
Zhu, H., Kavsak, P., Abdollah, S., Wrana, J. L. and Thomsen, G. H. (1999). A SMAD ubiquitin ligase targets the BMP pathway and affects embryonic pattern formation. *Nature* **400**, 687-693. doi:10.1038/23293
Zi, Z., Feng, Z., Chapnick, D. A., Dahl, M., Deng, D., Klipp, E., Moustakas, A. and Liu, X. (2011). Quantitative analysis of transient and sustained transforming growth factor-beta signaling dynamics. *Mol. Syst. Biol.* **7**, 492. doi:10.1038/msb.2011.22
Zi, Z., Chapnick, D. A. and Liu, X. (2012). Dynamics of TGF-beta/Smad signaling. *FEBS Lett.* **586**, 1921-1928. doi:10.1016/j.febslet.2012.03.063